Princeton Plasma Physics Laboratory

Mitigation of Alfvenic activity by 3D magnetic perturbations on NSTX

G.J. Kramer[1], A. Bortolon[1], N.M. Ferraro[2,1], D.A. Spong[3],
N.A. Crocker[4], D.S. Darrow[1], E.D. Fredrickson[1], S. Kubota[4],
J-K. Park[1], M. Podesta[1], W.W. Heidbrink[5], and the NSTX Team

[1]Princeton Plasma Physics Laboratory, P.O.Box 451, Princeton, New Jersey 08543, USA
[2]General Atomics, P.O. Box 85608, San Diego, California 92186, USA
[3]Oak Ridge National Laboratory, Oak Ridge, Tennessee, USA
[4]University of California, Los Angeles, CA 90095, USA and
[5]University of California, Irvine, CA 92697, USA

February 2016

PRINCETON PLASMA PHYSICS LABORATORY

Princeton Plasma Physics Laboratory
Report Disclaimers

PPPL Report Availability

Princeton Plasma Physics Laboratory:

http://www.pppl.gov/techreports.cfm

Office of Scientific and Technical Information (OSTI):

http://www.osti.gov/scitech/

Related Links:

U.S. Department of Energy

U.S. Department of Energy Office of Science

U.S. Department of Energy Office of Fusion Energy Sciences

Mitigation of Alfvénic activity by 3D magnetic perturbations on NSTX

G.J. Kramer[1],[*] A. Bortolon[1], N.M. Ferraro[2,1], D.A. Spong[3],

N.A. Crocker[4], D.S. Darrow[1], E.D. Fredrickson[1], S. Kubota[4],

J-K. Park[1], M. Podestà[1], W.W. Heidbrink[5], and the NSTX team

[1]*Princeton Plasma Physics Laboratory,*

P.O.box 451, Princeton, New Jersey 08543, USA

[2]*General Atomics, P.O. Box 85608,*

San Diego, California 92186, USA

[3]*Oak Ridge National Laboratory, Oak Ridge, Tennessee, USA*

[4]*University of California, Los Angeles, CA 90095, USA and*

[5]*University of California, Irvine, Irvine, CA 92697, USA,*

(Dated: February 16, 2016)

Abstract

Observations on the National Spherical Torus eXperiment (NSTX) indicate that externally applied non-axisymmetric magnetic perturbations (MP) can reduce the amplitude of Toroidal Alfvén Eigenmodes (TAE) and Global Alfvén Eigenmodes (GAE) in response to pulsed n=3 non-resonant fields. From full-orbit following Monte Carlo simulations with the 1- and 2-fluid resistive MHD plasma response to the magnetic perturbation included, it was found that in response to MP pulses the fast-ion losses increased and the fast-ion drive for the GAEs was reduced. The MP did not affect the fast-ion drive for the TAEs significantly but the Alfvén continuum at the plasma edge was found to be altered due to the toroidal symmetry breaking which leads to coupling of different toroidal harmonics. The TAE gap was reduced at the edge creating enhanced continuum damping of the global TAEs, which is consistent with the observations. The results suggest that optimized non-axisymmetric MP might be exploited to control and mitigate Alfvén instabilities by tailoring the fast-ion distribution function and/or continuum structure.

---
[*]gkramer@pppl.gov

I. INTRODUCTION

As the fusion program develops in support and preparation of burning plasma operation, the role of fast ions is becoming central for scenario development. Not only is proper confinement of energetic ions from neutral beam injection (NBI) key for heating but it also enables the use of beam ions for current drive, and hence better control of magnetic safety factor or q profile. Concerns exist for the rapid loss of energetic ions induced by Alfvénic instabilities, that may jeopardize the plasma performance or, if localized, it can damage vessel components [1, 2].

In magnetic confinement devices Alfvénic instabilities are commonly observed which are often driven by the fast-ion population itself and manifest themselves with a strongly non-linear dynamic, characterized by bursting and frequency-chirping [3, 4]. Those instabilities can span multiple frequency bands up to the ion-cyclotron frequency and have been observed in tokamaks, spherical tokamaks, and stellarators in which energetic-particle populations are created with, among others NBI, ion-cyclotron and electron-cyclotron heating. Coupled "avalanches" of multiple bursting modes were also observed [5] and in many cases accompanied by substantial fast ion losses.

To maximize the performance of a fusion device, viable methods to suppress or mitigate the effect of such modes are highly desirable. Since instabilities grow to a finite size when the growth rate exceed the damping rate, the mitigation or suppression of AEs can be achieved by reducing the drive for the instability or by enhancing the damping mechanism. As the chirping dynamic is in some cases associated with coherent structures that propagate in phase space, mitigation could also be achieved by interfering with the formation and/or propagation of such structures.

In several experiments the mitigation of energetic-particle driven instabilities was obtained with different forms of auxiliary wave heating. In an experiment performed in a small magnetic dipole device [6, 7], the application of electron cyclotron waves to the energetic electrons that were driving violent, bursting, rapidly-chirping interchange modes converted the modes into a smaller amplitude mode of nearly constant frequency. Electron cyclotron heating was tested in DIII-D as possible tool to control reversed shear Alfvén eigenmodes, finding reduced activity when EC power was deposited near the location of reversal of safety factor shear [8]. More recently, in the stellarator TJ-II observations of strong impact of EC

heating on non-linear behaviour of Alfvén modes were reported, up to complete suppression [9]. During periods of fast-wave heating, reduction or suppression of Alfvénic activity has been reported in NSTX [10–12]. While some of these observations could be interpreted as scatter of coherent phase space structures [6, 7, 10], it is extremely challenging to draw conclusions about the mechanisms responsible for the observed behaviour. This is partly due to the difficulty of developing actuators that affect a single aspect of the mode dynamic, i.e. a specific mechanism for driving or damping modes.

Mitigation can be achieved indirectly, for example when Alfvénic instabilities are coupled with other MHD activity as was observed among other on JT-60U [13] and TFTR [14]. An example is the occurrence of core-localized Toroidicity-induced Alvén eigenmodes (TAE) before and Ellipticity induced Alvén eigenmodes after giant sawtooth crashes [15]. By using electron cyclotron waves to reduce the amplitude and increase the frequency of sawtooth crashes the TAEs can be suppressed [16].

A novel method to manipulate and control the Alfvén Eigenmode AE activity is by using external applied static three-dimensional magnetic perturbation (MP) fields [18]. Extensive modeling suggested that a reduction of the fast-ion drive for the instabilities could be responsible for the mitigation observed in these scenarios. The study of the role of fast-ion transport in the perturbed equilibria requires accounting for the plasma response to the applied 3D fields. The plasma response as obtained from the ideal MHD code IPEC [17] was used to address the role of fast-ion transport due to MP fields in NSTX. In this paper we further extend the investigation of the fast-ion drive in these scenarios with the inclusion of the resistive MHD plasma response to the applied 3D magnetic perturbation. This allows for a more accurate modeling of the fast-ion transport and a more quantitive comparison can be made with the experimental results.

The role of enhanced continuum damping as a possible mechanism for the observed reduction of Toroidal Alfvén Eigenmodes in presence of n=3 static fields on NSTX is also explored in this paper by determining the 3D Alfvén continuum for the 3D perturbed equilibrium using 3D codes that were developed for stellarators.

The remainder of the paper is organized as follows: the experimental evidence for mitigation of TAE and GAE in discharges with pulsed MP is presented in section II. In section III the simulations that were performed to determine the plasma response to applied MP and time dependent transport of fast ions induced by the total perturbation fields is presented
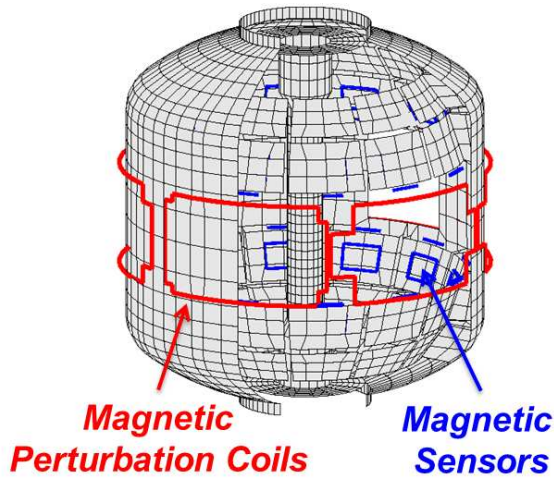
3

FIG. 1: The location of the six magnetic-field perturbation coils at the outside of the NSTX vacuum vessel. The magnetic sensor coils are located inside the vessel.

for the relevant experimental cases. Possible effects of changes of the distribution function and toroidal mode coupling associated with the MP on the AE stability are studied in section IV while a summary of the results and a perspective for the use of this technique in fusion devices is presented in the concluding section.

II. EXPERIMENTAL METHODS AND RESULTS

The observations discussed in this work were obtained in experiments conducted on the National Spherical Tokamak experiment (NSTX) [19]. NSTX is a medium size device (major radius $R = 0.85$ m, minor radius $a \approx 0.6$ m, elongation $\kappa = 1.8 - 2.2$), that operates at toroidal magnetic fields of $B_t = 0.3$-0.5 T and plasma currents up to $I_p = 1$ MA. Neutral Beam injection (NBI) is the main auxiliary heating system, composed of three independent sources with adjustable acceleration energy, E_b, between 60 and 90 keV, delivering a maximum total injected power of $P_{NBI} = 7$ MW. The three beam lines inject deuterium neutrals in the direction of the plasma current with tangency radii of $R_{tan} = 0.7$, 0.6 and 0.5 m, providing the main source of the non-thermal ion population. NSTX is equipped with a system of six two-turn coils that produce static magnetic-field perturbations. The coils are located at the equatorial plane (see Fig. 1). Coil pairs can be energized separately, to obtain perturbing fields with dominant toroidal periodicity n=1,2 or 3.
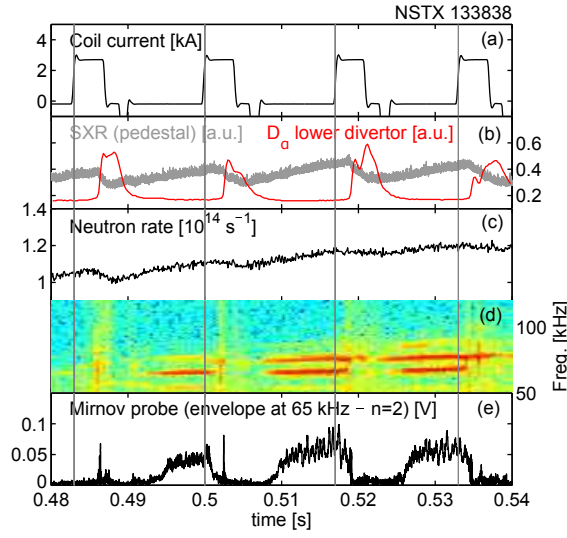
FIG. 2: time traces from a NSTX discharge with ELM-pacing by applied n=3 MP. (a) MP coil current. (b) D_α emission from the divertor and soft X-ray emission from a chord traversing the pedestal. (c) The neutron production rate. (d) The effect of n=3 MP on TAEs is visible on the Mirnov coil spectrogram. (e) The Mirnov signal at the TAE frequency reduces strongly after the coil current is ramped up and before the ELM crash.

Since the velocity of beam ions are up to five times the Alfvén velocity, fast ions provide a strong drive for different types of Alfvénic instabilities that develop throughout the discharge. In this study the AE instabilities were excited by fast ions from the 90-kV deuterium NBI neutrals that were injected into an ELM-free H-mode plasma with lithium-coated carbon walls [20]. Traces from two representative discharges ($I_p = 900$ kA, $B_t = 0.35$ T) are shown in Figs. 2 and 3. During the flat-top phase the beam power and plasma current are constant while the electron density steadily increases from 4 to 8 $\times 10^{19}\,\mathrm{m}^{-3}$.

A.   Mitigation of low frequency TAE

Mitigation of TAE activity was observed for non-chirping TAEs in H-mode plasmas where pulsed n=3 fields were utilized to pace ELMs. The modes were visible (NSTX pulse 133838) in a spectrogram of a magnetic probe (Fig. 2d) showing a cluster of coherent fluctuations at frequencies between 60 and 90 kHz which are Doppler-shifted TAEs with toroidal numbers n=2 (60 kHz), n=3 (70 kHz), and n=4 (80 kHz). From reflectometer density fluctuation measurements, a radial displacement of 0.14 mm was found in the plasma edge for the
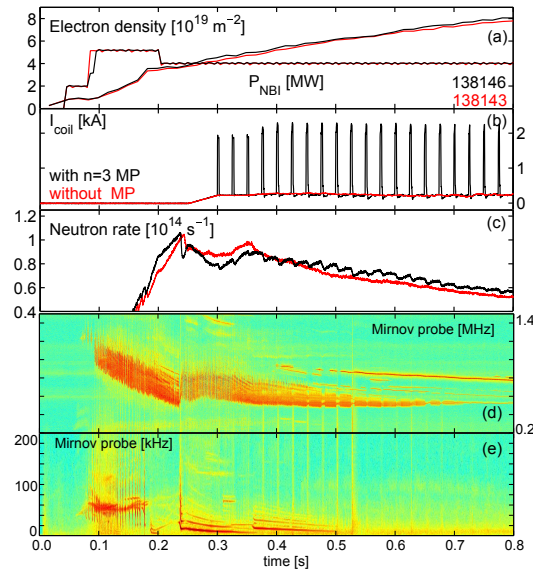
FIG. 3: Time traces from two NSTX discharges with (red) and without (black) applied n=3 MP. (a) Line integrated electron density and injected neutral beam power, (b) MP coil current, (c) the neutron production rate. Mirnov coil spectra in the (d) TAE frequency range (0-200 kHz) and (e) GAE/CAE frequency range (0.2-1.4 MHz). The effect of the n=3 MP on the GAEs is visible after 0.4 s, as a modulation of the broad band activity in the 450-650 kHz frequency range. (Frames a, b, and c were shown first in [18]).

n=2 mode. The density fluctuations could not be measured with reflectometry beyond the pedestal because of the hollow density profile which is characteristic of NSTX H-modes. Ideal MHD computations with the NOVA code [21] indicate that the TAE gap is open up to the last closed flux surface when no MP fields are present. These simulations also showed that these are global TAEs [22] stretching from well inside the plasma to the edge whereby a large number of poloidal harmonics couple to create a finite TAE amplitude at the edge.

In response to the applied n=3 MP fields the TAE amplitude drops rapidly as can be seen on the Mirnov coil signal in Figure 2(e) which is band-pass filtered around the n=2 mode frequency. The n=2 signal decreases rapidly after the MP coils are energized but before the ELM crash which occurs approximately 2 ms after the coil current is stepped up. Notice that there is no increase in the neutron signal when the TAE amplitude is reduced due to the MP fields except for pulse at 0.50 s where the TAE amplitude is small and the MP fields are successful in suppressing the mode fully.

6

B. Mitigation of high frequency GAE

In discharge 138146 a MP configuration with toroidal periodicity $n = 3$ was employed with coils pulses of 3 ms long and a repetition rate of 40 Hz. The coil current amplitude was chosen to be just below the threshold for repetitive triggering of ELMs ("ELM pacing" [23]). In discharges such as the one shown in Fig. 3, ELM pacing does not occur, and the plasma remains virtually ELM-free. The coil pulses, however, cause rapid $\lesssim 8\%$ reductions in the volume-integrated neutron emission whose secular decrease is associated with deuterium dilution from carbon accumulation. For these conditions, the neutron rate is dominated by beam-plasma reactions so the neutron reduction indicates a degradation of the fast-ion confinement.

Persistent bursting modes at frequencies between 400-700 kHz were detected on magnetic probes in these discharges. The modes have toroidal mode numbers of $n = 7 - 9$ and based on their mode numbers and frequency evolution [24] are thought to be Global Alfvén Eigenmodes (GAE) [25]. Both GAEs and Compressional Alfvén Eigenmodes (CAE) [26] can be present in NSTX in the 0.5 to 2.0 MHz frequency range with very similar experimental characteristics but CAEs need a potential well [27] which is not present at the experimental parameters of the observed mode and therefore, we identify those modes as GAEs. CAEs were observed in this discharge before 0.3 s around 2 MHz but ceased to exist after 0.3 s. In the absence of MP fields the GAEs exhibit a bursting and chirping behavior with a bursting rate of ~ 4 kHz and a frequency sweep of ~ 100 kHz (Fig. 4).

When the MP fields are applied the frequency sweep, repetition period, and mode amplitude all drop by a factor of 2-3. Those effects occur in ~ 0.1 ms which is the typical poloidal transit timescale and is much shorter than the timescale for the formation of a fast-ion slowing-down population which occurs on the collisional time scale of the energy slowing down time of about 20 ms. In contrast, when the MP current is turned off the bursting stays small for several milliseconds which is typical for the NBI refueling timescale. In this case the mitigation effects are decoupled from the ELM behavior and are most readily observed during ELM-free phases of the discharge. Edge soft x-ray signals are barely perturbed by the MP pulses suggesting that the MP have a minor effect on the plasma edge density and temperature profiles leaving the beam deposition unaltered.

The phenomena shown in Figs. 3 and 4 are observed consistently in a set of 20 discharges
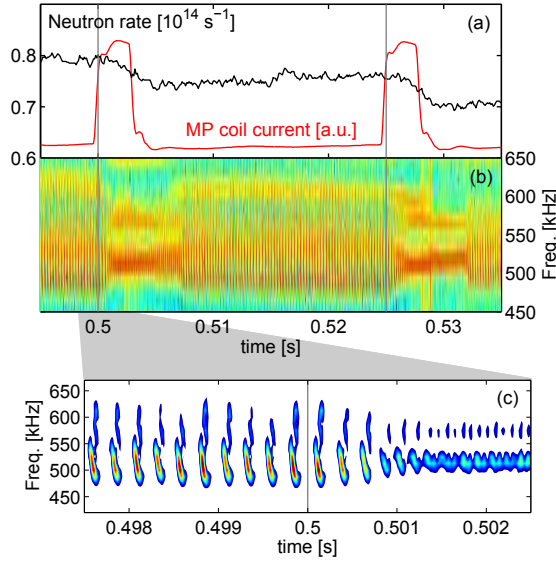
FIG. 4: (a) Applied n=3 MP pulses (red) are followed by rapid reduction of the neutron yield and (b) a substantial change in the character of the GAE activity is observed on the Mirnov coil signals. (c) A high resolution spectrogram of Mirnov coil signal shows a clear reduction in the bursting and chirping character of multiple modes when the MP fields are applied at 0.5 s. (Figure was shown first in [18]).

of this type, with variable MP duration (2-6 ms), repetition rate (20-40 Hz) and coil current (0.8-2.2 kA per turn). Pulses with MP coil currents below 1 kA per turn have little or no effect. Concurrent, large-amplitude, low-frequency MHD masks or weakens the mitigation effect.

In contrast to the TAE case, a clear reduction in the neutron rate is observed in response to applied 3D fields, in discharges with only high-frequency GAE and CAE activity. This suggests that the fast-ion distribution in the discharges with TAE activity is already affected by the modes in such a way that any additional changes to the fast-ion population due to the MP fields are not detectable.

III. SIMULATIONS

In order to understand the effects of MP fields on the fast ions as presented in the previous section we have used state-of-the-art simulations with experimental equilibrium profiles as input for NSTX discharge 138146 (figs. 3 and 4). The results of these simulations can be
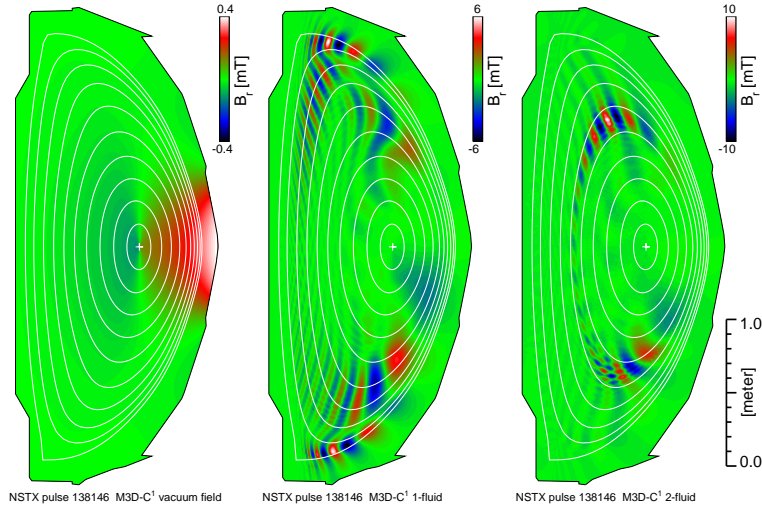
FIG. 5: The radial component of the n=3 (a) vacuum field, (b) the one-fluid, and (c) the two-fluid plasma response as calculated with M3D-C^1. Note that the color scale changes from ± 0.4 mT in (a) to ± 6 mT in (b) and ± 10 mT in (c).

compared directly with observations. We have chosen to study the changes in the fast-ion population in this NSTX discharge at 0.5 s because it is free of low-frequency TAE activity which is known to be able to redistribute fast ions efficiently [28] and hence, mask the effects of the MP fields on the fast ions. The high frequency CAE and GAE activity that is visible on the Mirnov coil signals (Fig. 3) is not harmful for the fast-ion population because they are weak despite their visibility. Mirnov coils are sensitive to the time derivative of the magnetic fluctuations and therefore, the signals are linearly weighted to high-frequency activity.

The equilibrium reconstruction used as input for the resistive 1- and 2-fluid M3D-C1 calculations [29–31] was computed with the EFIT code [32] and included the effects of kinetic profiles. The vacuum n=3 MP fields were obtained from a Biot-Savart calculation for the currents in the MP coils in NSTX. The vacuum fields are rather small and localized at the low-field side mid-plane as is shown in Fig. 5a. The one- and two-fluid plasma responses, however, are strong as is shown in Figs. 5b and c. In the one-fluid case the $\mathbf{E} \times \mathbf{B}$ rotation changes sign at two places near the plasma edge (Fig. 6a) where the internal kink response is strong. Similarly, in the two-fluid simulations the electron diamagnetic frequency changes sign near $r/a = 0.6$ resulting in a strong kink response there as can be seen from the flux surface averaged magnetic perturbation shown in Fig. 6b.

The fast-ion distribution was created in the simulation by continuously injecting the
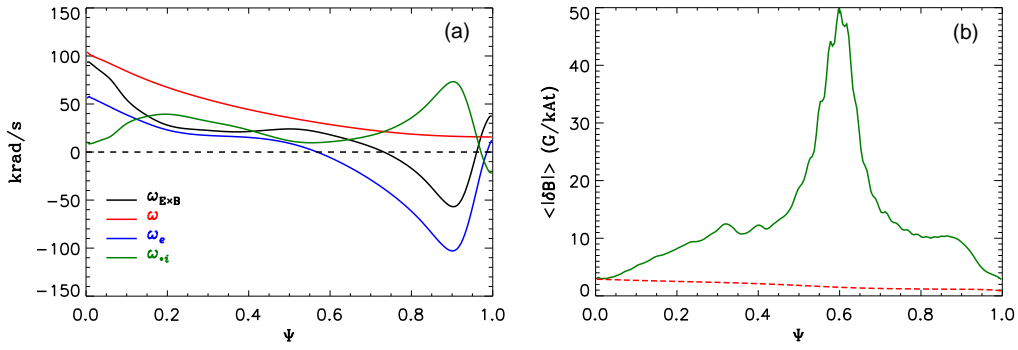
9

FIG. 6: (a) Radial profiles of the $\mathbf{E} \times \mathbf{B}$ frequency (black), the plasma rotation frequency (red), the electron and ion diamagnetic frequencies (blue and green) used in the M3D-C1 simulations of the two-fluid plasma response. The quantities were derived from the measured pressure and rotation profiles and used as an input for the simulations. (b) Flux-surface averaged magnetic perturbation for the vacuum field (dashed) and two-fluid plasma response (solid).

three energy components of two neutral beams with full energies of 90.0 and 89.5 keV. These ions then slow-down and scatter on the bulk plasma when they thermalize with a typical energy slowing-down time of 25 ms forming a slowing-down distribution. In the simulations the slowing-down distribution was calculated with the SPIRAL code [33] from the fast-ion deposition profiles that included the full, half, and third energy components as calculated with the NUBEAM package in the TRANSP code [34, 35] resulting in a typical $(v_\parallel, v_\perp)$ distribution as shown in Fig. 7 whereby the parallel and perpendicular velocity components are taken at the particle location. In this representation of the fast-ion velocity space particles with constant energy form semi-circles while particles with constant pitch are on straight lines going through the origin. The advantage of using the $(v_\parallel, v_\perp)$ phase space representation over the more commonly used (energy,pitch) representation is that TAE and counter-propagating GAE resonances for passing particles are straight lines at constant $v_\parallel$.

The slowing-down distribution was generated in the simulations by drawing particles from the birth profiles and injecting them at a constant rate of 8000 particles per ms and in a 25 ms time interval. Those particles were then followed until 25 ms or until they got lost to the wall or reached thermal velocities. The resulting ensemble of confined particles is then representative of the slowing-down distribution before the MP turns on. The effects of the MP fields on the fast ions was then studied by introducing the 3D perturbed magnetic fields from different models and continuing the simulations with the same constant fueling rate
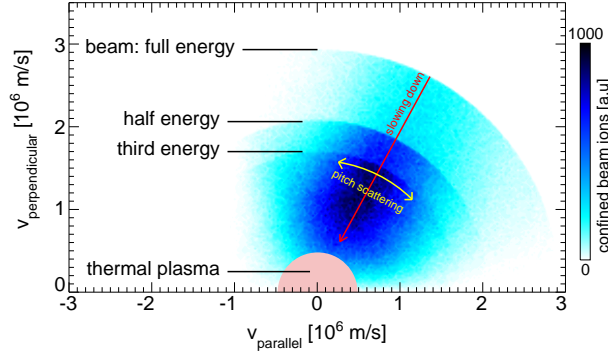
10

FIG. 7: Fully develloped fast-ion slowing-down distribution integrated over the total plasma volume in $(v_{\parallel}, v_{\perp})$ phase space where particles with constant energy form semi-circles and the angle is the particle pitch. Energy slowings-down follows radii of constant pitch (red arrow) and pitch angle scattering occurs at semi-circles with constant energy. The full, half, and third energy components are indicated. The thermal plasma is located at the pink semi-circle near the origin.

as before whereby the fast-ion distribution was recorded at regular time intervals (0.2 ms) for further analysis. In all SPIRAL calculations, the full particle orbit was calculated (i.e. including gyro-motion) because the typical size of the perturbed fields is on the order or smaller than the fast-ion Larmor radius. Moreover, because of the low equilibrium magnetic fields in spherical tori, the criteria for applicability of guiding-center models are not well satisfied, as was shown in [36].

Linear calculations were performed with the M3D-C[1] code therefore the vacuum and plasma response fields were known up to an arbitrary scaling factor. Moreover, the MP coils are located outside the vacuum vessel and it takes on the order of 5 ms for the perturbing fields to penetrate fully into the vacuum vessel. This wall response time is on the same order of the duration of the applied pulses in the experiment (3 to 5 ms). In order to get a realistic time behavior of the perturbed fields inside the vessel and in the plasma we have normalized the fields as obtained from M3D-C1 to the signal of a magnetic probe that was located inside the vacuum vessel and far from the plasma so that it only registered the vacuum field response. The distortions of the in-vessel perturbed magnetic fields due to the vacuum vessel response time can be seen clearly in Fig. 8a where the probe response is compared with the applied MP coil current. The plasma response is scaled with the same factor because the plasma response occurs on the Alfvénic time scale of about 10 μs. Simulations were
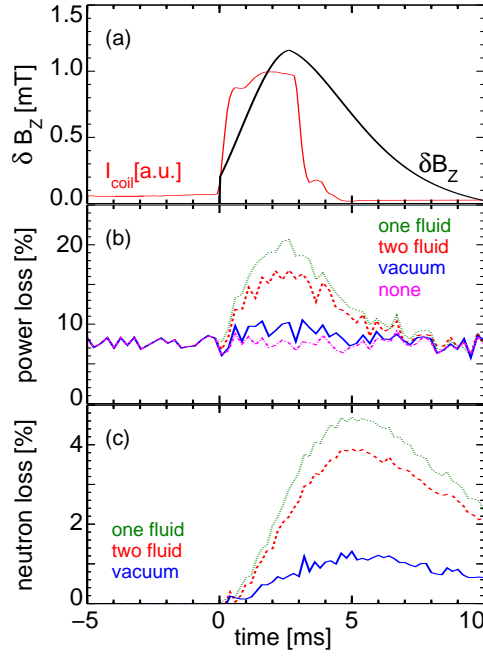
FIG. 8: (a) The coil current applied outside the vacuum vessel and the magnetic field response inside the vacuum vessel away from the plasma so that it only registered the vacuum field response. (b) Simulated power loss without (purple, dash-dotted) MP field and with only the vacuum response (blue, solid), and the one-fluid (green, dotted) and two-fluid (red, dashed) response. (c) Simulated neutron loss for the vacuum (blue, solid), one-fluid (green, dotted) and two-fluid (red, dashed) response.

performed for four cases: 1) with no MP fields, 2) with the vacuum response only, 3) with the one-fluid plasma response and 4) two-fluid plasma response.

When the MP fields are applied the fast-ion losses increase from the prompt-loss level of 8% of the injected power to transiently up to 21% at the end of the current pulse (Fig. 8c). This transient occurs because the MP fields increase the loss cone in phase space thereby ejecting marginally confined particles. In this case, the coils were switched off before a new phase-space equilibrium with the MP fields included was established. After the coils were switched off the enhanced losses disappear on a time scale comparable to the decay rate of the perturbed fields.

The MP induced losses are small (up to 2%) for the vacuum fields only and increase significantly (up to 12 and 8%) when the one- or two-fluid plasma response is included. The MP-induced fast-ion losses occur mainly at the low-field side mid-plane in a n=3 pattern
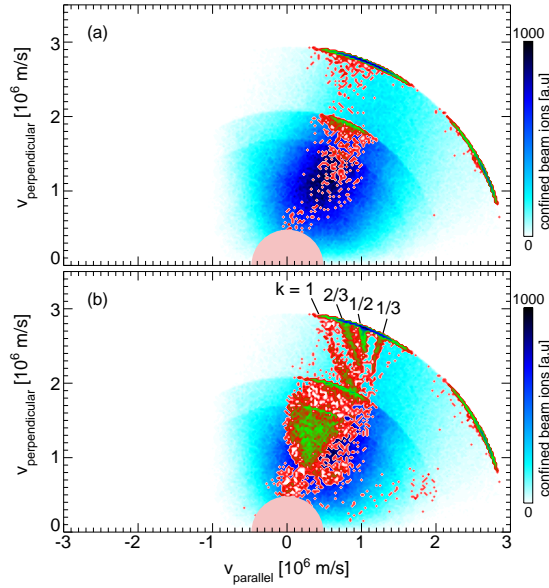
12

FIG. 9: Fast-ion loss regions in $(v_\parallel, v_\perp)$ phase space (a) without and (b) with the n=3 magnetic perturbation fields present. The losses increase from red to green. Resonant losses visible in (b) and are marked with their respective bounce harmonic number, k.

which is quite different from the MP-induced losses on conventional tokamaks where the losses occur in the lower divertor region [37]. The low equilibrium fields in NSTX give rise to significantly outward shifted co-going orbits and in combination with large Larmor radii, particles on those orbits are easily lost at the LFS mid-plane and don't reach the strongly perturbed fields near the X-points. In conventional tokamaks the outward orbit shift and Larmor radii are much smaller and the fast ions can reach the perturbed fields near the X-point where they become ripple trapped and lost to the divertor.

Without the MP fields present the losses in phase space occur mainly at the full and half energy components as prompt losses as can be seen in Fig. 9a. Once confined, the pitch angle scattering is small enough not to induce additional significant losses. When the MP fields are present, however, resonant losses occur for high-energy particles between the full and half energies while diffusive losses become dominant below the half energy component as can be seen in Fig. 9b. Note also that without MP fields the third-energy component which is deposited close to the edge is well confined but when the MP fields are present a significant amount of third-energy particles are lost.

The resonant condition for fast ions with the applied static MP fields can easily be
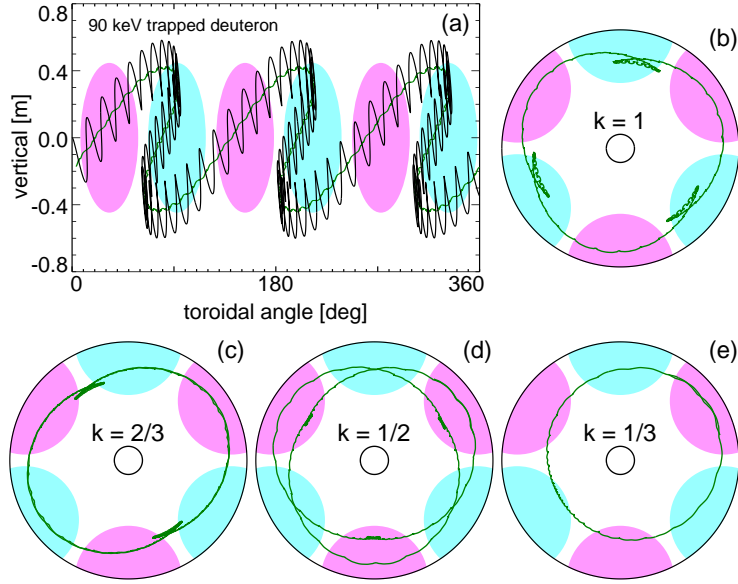
13

FIG. 10: (a) The projection of a resonant 90 keV deuteron on the toroidal angle, vertical plane. The black line is the full orbit projection while the green line is the (instantaneous) guiding center location. The red (blue) ovals indicate the radially inward (outward) pointing magnetic n=3 perturbation. (b-d) Top view of the guiding centers for the four resonant orbits (labeled with their respective bounce harmonic number) that were identified in the simulations.

deduced graphically from Fig. 10a as:

$$\frac{\omega_b}{\omega_p} = k\,n \tag{1}$$

with ω_b the particle bounce and ω_p the particle precessional frequency and k, a (rational) bounce harmonic. When inspecting the orbits of the resonant particles we find three resonant trapped particle orbits with $k = 1, 1/2$, and $2/3$ and one passing particle orbit with $k = 1/3$ as shown in Fig. 10 and indicated in Fig. 9b.

The changes in the neutron rate can be calculated from the simulated confined fast-ion distribution and the thermal plasma profiles as measured with the NSTX Thomson scattring system [39, 40] by using some elementary equations for the energy-dependent deuteron-deuteron cross sections as given in [41]. In contrast to the fast-ion losses which peak at the maximum of the perturbed field amplitude, the neutron losses peak 5 ms after the perturbation was applied (Fig. 8c) while the neutron rate recovers on the slowing-down time scale which is in good agreement with the measurements (Fig. 11). The amplitude
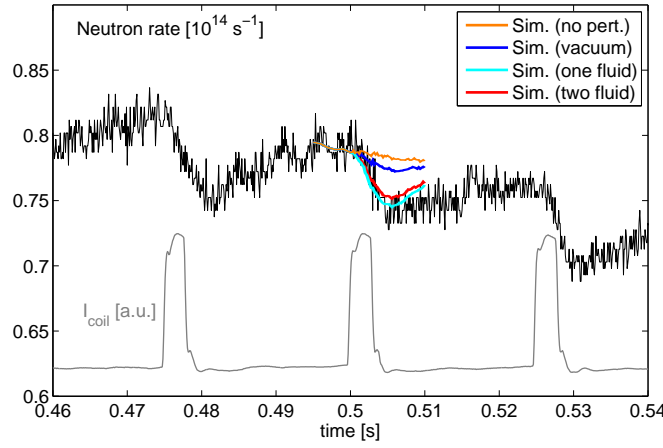
14

FIG. 11: The measured neutron rate (black) compared with SPIRAL simulation without perturbation (yellow) and with the vacuum MP only (blue) and the one-fluid (cyan), and two-fluid (red) plasma response included. In gray the MP pulses are indicated.

of the predicted neutron rate drop depends significantly on the perturbed fields that were used. When only the vacuum fields are included the peak neutron loss is 1% which is six times lower than the observed one while the one- and two-fluid plasma response fields give losses that are comparable to the observed ones as can be seen in figs. 8c and Fig. 11. Ideal MHD computations of the plasma response using the IPEC code [17] that were reported in [18] found a larger MP amplitude in the core, which resulted in an overestimate of the simulated neutron rate drop. Hence, the inclusion of resistivity effects provides a more accurate representation of the plasma response in this scenario. Therefore, we conclude that for simulating meaningful MP-induced loss rates the resistive plasma response has to be included for low-n MP fields.

IV. EFFECTS OF MP FIELDS ON AES

It was found experimentally that applied MP pulses can affect the dynamic of fast-ion driven TAEs and GAEs (Fig. 2 and 4). The resonant drive for TAEs from passing particles is given by $v_\parallel/v_A = 1$ and a side band at $v_\parallel/v_A = 1/3$ with v_A the Alfvén velocity [38]. For trapped particles the resonant drive emerges when the TAE frequency, ω_{TAE}, equals $\omega_p + j\,\omega_b$ with ω_p the precession frequency, ω_b the bounce frequency, and j an integer bounce harmonic. The drive for the high-frequency counter-propagating GAEs as were observed

15

in the experiments comes from particles that satisfy the GAE resonant condition: $\omega_{\text{GAE}} = k_\parallel v_\parallel + l\,\omega_{ic}$ that, together with the dispersion relation for Alfvén eigenmodes, $\omega_{\text{AE}} = k_\parallel v_A$, leads to $v_\parallel / v_A = 1 - l\,\omega_c / \omega_{\text{GAE}}$ with ω_c the ion cyclotron frequency, ω_{GAE} the GAE frequency and l an integer bounce harmonic. The wave passing-particle resonances for the TAEs and for the GAEs emerge as straight lines in $(v_\parallel, v_\perp)$ phase space.

In the following we will use semi-qualitative arguments to show how the MP fields can influence the TAE and GAE activity via changes in the fast-ion phase space distribution to reduce the AE drive. For GAEs this change in drive is the major factor for the observed change in activity but for TAEs changes in the continuum damping rate at the plasma edge due to the MP fields can also contribute to the observed TAE suppression.

The bursting and chirping behavior of modes such as the observed GAE (Fig. 3) is often ascribed to the eruptive dynamics which is characteristic of marginally stable modes: modes for which the total growth rate only slightly exceeds the total damping rate [44]. Under such conditions one can expect that relatively small changes of the drive or damping, possibly caused by the interaction of the mode with the fast-ion distribution, might alter significantly the non-linear dynamics of the mode. Although those non-linear physics mechanisms are studied extensively (see [45, 46] and references therein), direct comparisons between theory and experiments are still sparse because accurate measurements of the fast ions in phase space are lacking. In the following we investigate whether the fast-ion transport can be changed sufficiently with externally applied 3D fields to alter the GAE drive significantly.

For the observed GAE the resonances include the $l = 0$ resonance which intersects the passing particle population marginally in the core and not in the edge as is shown in figs. 12 a and b while the $l = -1$ resonance intersects both the core and edge passing-particle population. When the MP fields are applied the passing particle distribution changes in the core and at the edge as can be seen in figs. 12c and d when the one-fluid plasma response is taken into account and in figs. 12e and f for the two-fluid response. For both the one and two fluid response a depletion of the distribution is found in the core for $v_\parallel < 10^6$ m/s while at the edge the passing particle distribution is enhanced.

The GAE instability depends on the perpendicular-velocity space gradient of the distribution function along the resonance as was shown in [25]. The phase space distributions along the $l = -1$ resonance (at $v_\perp = 2.08\,10^6$ m/s) are shown in Fig. 13a and b for the core ($r/a < 0.6$) and the edge ($r/a > 0.6$) respectively where it can be seen that both the one
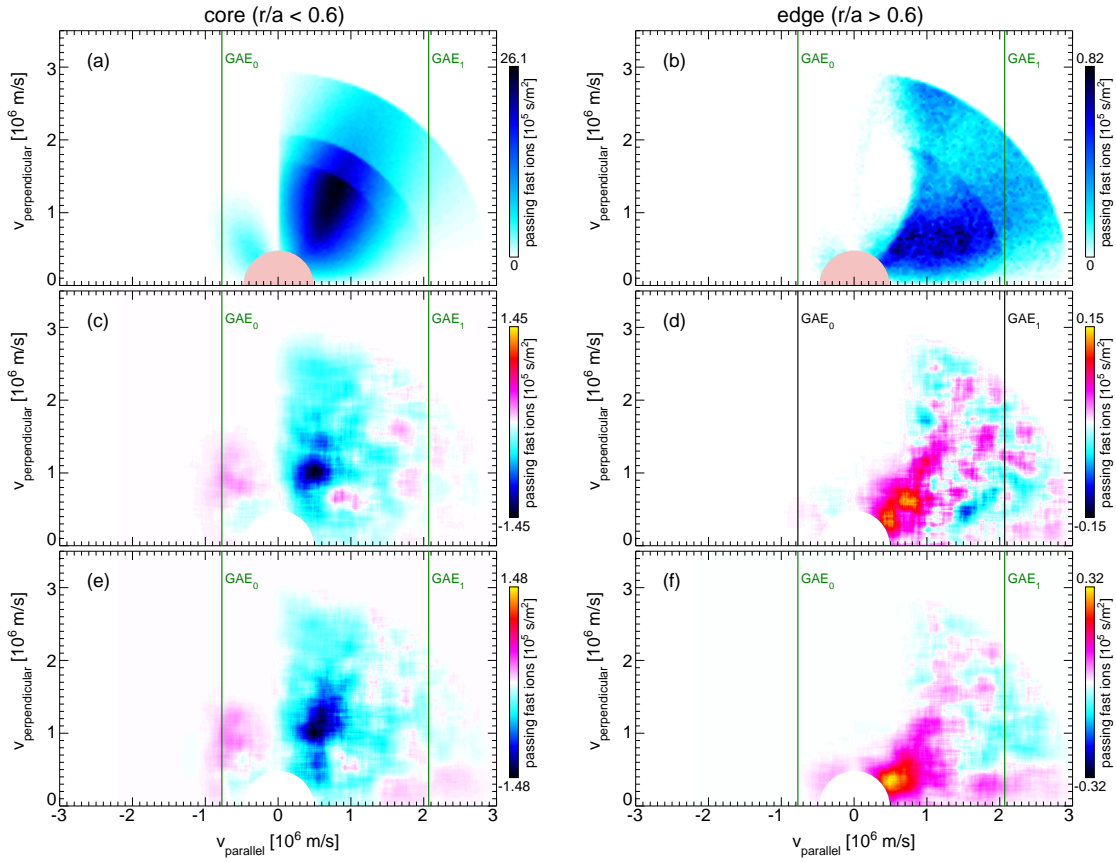
16

FIG. 12: $(v_\parallel, v_\perp)$-phase space distribution for passing particles (a) in the core and (b) in the edge. Changes in the passing particle distribution for the one-fluid pertubation (c) in the core, (d) in the edge and for the two-fluid perturbation (e) in the core and (f) in the edge. Blue colors in (c-f) indicate depletion while red colors show an increase in the passing particle population.

and two fluid response modify the distribution. For the excitation of the GAEs the perpendicular velocity gradient, $\partial F / \partial v_\perp$, is the determining factor. Compared to the unperturbed gradient both the gradients for the one and two fluid are reduced in the core and at the edge as is shown in figs. 13c and d, indicating that the MP fields can reduce the GAE fast-ion drive. Trapped particles can resonate with the GAE [25] when $v_\parallel / v_A > (1 + \omega_C / \omega_{\text{GAE}})$ but this condition is not satisfied in the current NSTX discharge.

For a quantitative analysis of the GAE drive the spatial distribution of the eigenmode in the plasma is needed and can be obtained from reflectometer measurements as was shown in [43]. Unfortunately, these measurements were not available in this experiment because of the steep edge density gradients and the flat or hollow density profiles in the core as is shown in Fig. 14 and therefore, an accurate quantitative estimate of the change in GAE
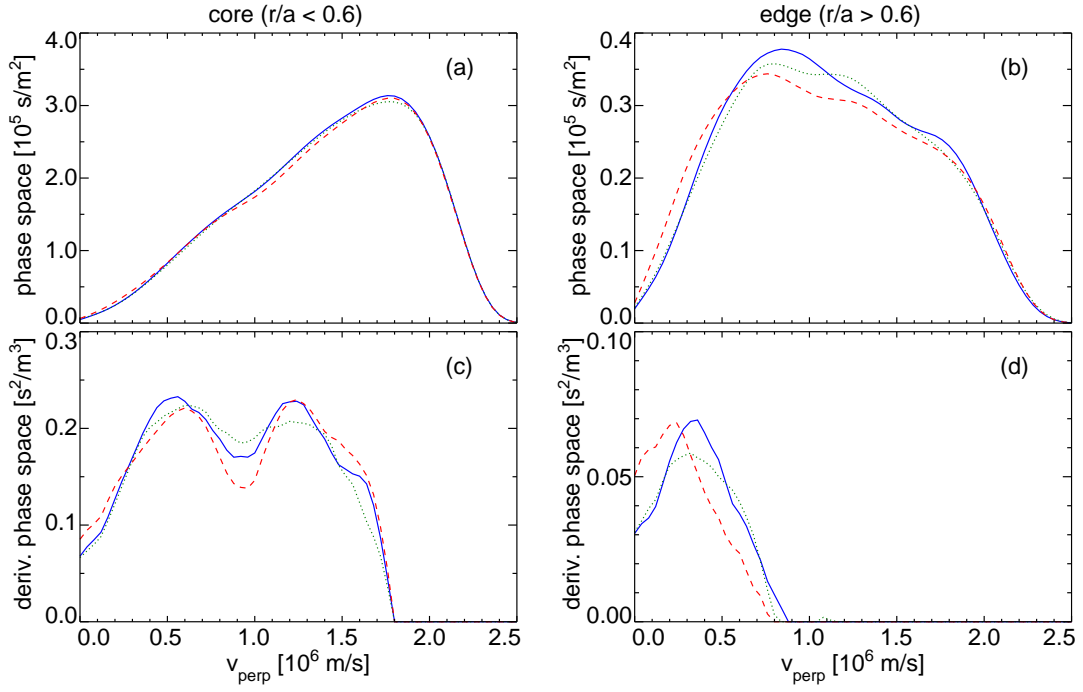
FIG. 13: Fast ion density along the GAE_1 resonance (a) in the core $(0 < \rho < 0.6)$ and (b) edge $(0.6 < \rho < 1.0)$ region. Positive part of the derivative with respect to $v_\perp$ along the resonance in (c) the core and (d) the edge. Blue (solid) unperturbed distribution, green (dotted) one-fluid, and red (dashed) two-fluid perturbations included.

fast-ion drive is not possible.

The applied MP fields can not only influence the drive due to changes in the fast-ion distribution but they can also affect the damping of the AEs in two ways. The kinetic profiles such as density, electron, and ion temperature profiles can be modified by the applied magnetic perturbations, especially in cases where the vacuum MP is strongly amplified by the plasma response. This can lead to changes in the Landau damping on thermal electrons and ions. However, in the present experiments the profile changes due to the MP fields are small as can be seen in Fig. 14 so it is unlikely that MP-induced profile changes modify the balance between drive and damping terms in a significant way.

A more direct damping mechanism emerges from the toroidal symmetry breaking of the MP fields. This symmetry breaking introduces a source for toroidal coupling. In a non-axisymmetric equilibrium the MHD equations cannot be solved for each toroidal Fourier component separately and the eigenmodes will emerge as a combination of multiple finite
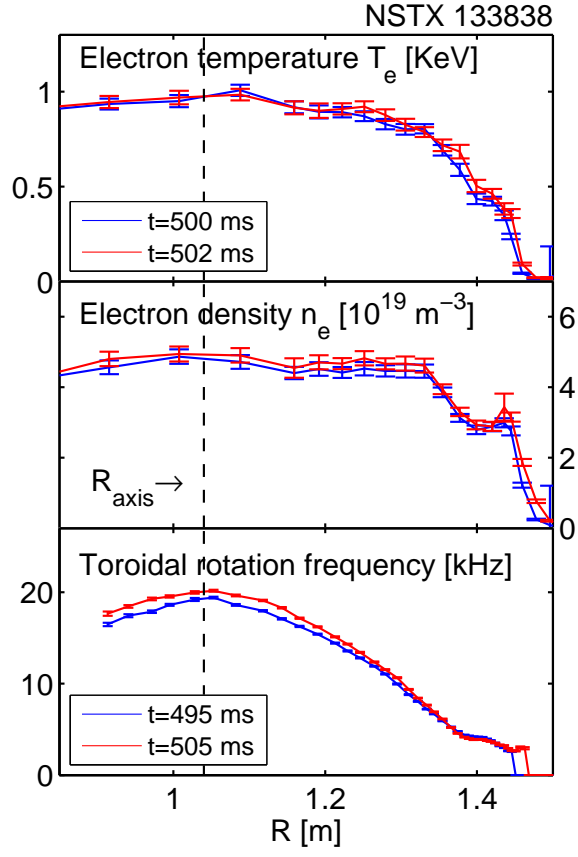
FIG. 14: Radial profiles of electron temperature and density and carbon toroidal rotation measured before (black) and during (red) a MP pulse. The vertical dashed line indicates the location of the magnetic axis.

toroidal and poloidal components. These aspects have been extensively studied for stellarators where due to the highly non-axisymmetric configurations perturbative methods are not viable [47].

In particular, the results in Ref. [47] imply that, when perturbing an axisymmetric equilibrium with MP fields of a low toroidal field period ($n_{MP} = 2, 3$), an eigenmode with toroidal number n_0 will generate a family of strongly coupled toroidal modes with mode numbers $n = \pm n_0 \pm k n_{MP}$ with $k = 0, 1, 2, ...$. Since this holds for the continuum solutions of the MHD equations as well, the application of external 3D fields is expected to alter the frequency, amplitude and radial extent of the Alfvén continuum gap structure.

To study this effect, the Alfvén continuum has been computed using the STELLGAP code [47] for a $n_{MP} = 3$ perturbed equilibrium corresponding to the experimental one of NSTX pulse 133838 at t=0.5 s just before the MP is applied. The 3-dimensional equilibrium
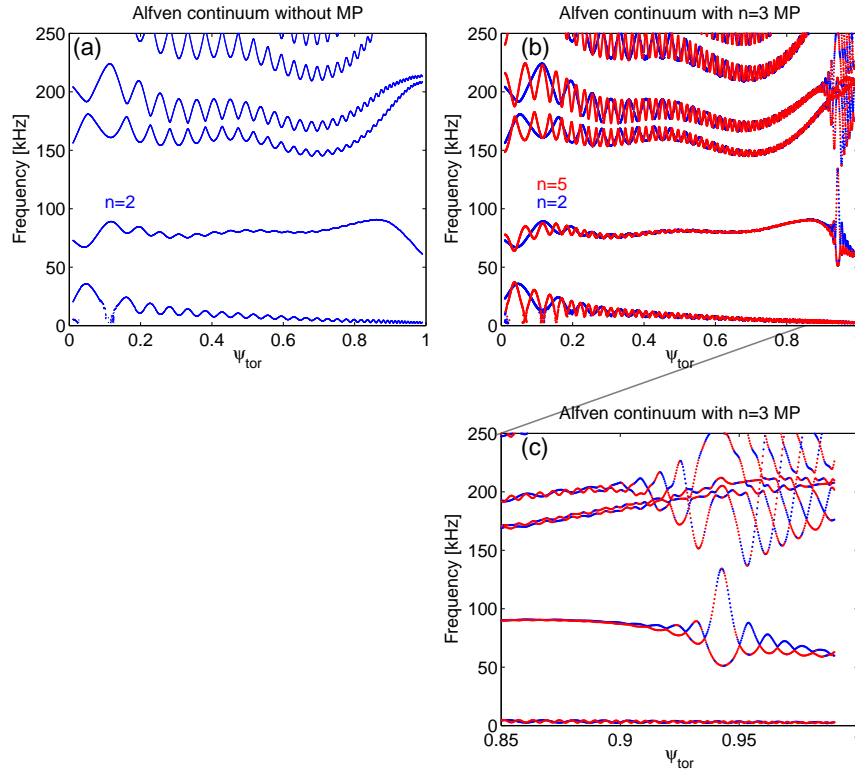
FIG. 15: (a) The axisymmetric n=2 Alfvén continuum and (b) the perturbed Alfvén continuum with toroidal coupling between the n=2 and n=5 modes due to the applied MP fields. (c) The perturbed Alfvén continuum at the plasma edge.

was calculated with the non-linear equilibrium code VMEC [48]. Two up-down symmetric VMEC equilibria were calculated by only including cosine-like terms in the representation of B and R and only sine-like terms included for Z. For the first equilibrium, only the $n = 0$ component of the fields was included in the computation, so as to provide an axisymmetric reference configuration. For the second equilibrium the $n = 3$ MP fields were included.

The structure of the n=2 continuum solutions without MP is shown in Fig. 15a where wide TAE (10-90 kHz) and EAE (100-150 kHz) gaps are found. When the $n_{MP} = 3$ MP are included, coupling between the $n = 2, 2 \pm 3, 2 \pm 6$, toroidal harmonics is expected. In figure 15b the continuum structure is shown, when the $n = 2$ and $n = 5$ components are included. In this figure the blue and red dots indicate continuum solutions with dominant toroidal component $n = 2$ or $n = 5$ respectively. The gap structure is strongly modified in a region close to the plasma edge in the H-mode pedestal region. It can be seen that the TAE gap is reduced and the EAE gap at the edge is closed due to 3D effects. This is due to the

presence of a new class of solutions (Figure 15c) that are characterized by finite $n = 2$ and $n = 5$ components, indicating a strong toroidal coupling in the pedestal region.

At present, the STELLGAP code does not include the effect of rotation which has been shown to be important for NSTX strongly rotating plasmas [49]. Hence, the results cannot be used for a direct quantitative comparison with the NSTX experiments. Nevertheless, it is interesting to notice that the upper bound of the TAE gap is reduced down to a frequency of 50 kHz, which suggest a possible interaction between the observed n=2 global TAE at 60 kHz with a finite amplitude near the plasma boundary and the MP-perturbed continuum. This suggests that the mode amplitude reduction of this global TAE might be attributed to a strongly increased continuum damping near the edge due to the MP fields.

V. DISCUSSION AND CONCLUSION

Suppression of Alfvén Eigenmode activity was observed when three-dimensional magnetic perturbation fields were applied on NSTX. Complete suppression of TAEs due to short MP pulses was observed whereas GAE activity was significantly reduced. Two mechanisms for the reduction of AE activity were identified, involving respectively changes in the fast-ion drive or continuum damping.

Extensive state-of-the-art full-orbit fast-ion modeling in which the plasma response to the MP fields was included has shown that the fast-ion distribution is affected in such a way that the drive for the observed GAEs is reduced. Simulations of the experimental scenario found that the inclusion of the plasma response as calculated with the resistive M3D-C[1] code was crucial to reproduce the measured drop in neutron production rate associated with the applied magnetic perturbations. Taking only the vacuum fields of the MP into account resulted in a simulated neutron rate drop that is more than four times smaller than the observed one whereas using ideal MHD to calculate the plasma response resulted in a significant over-estimate of the neutron rate drop. From full-orbit modeling with the SPIRAL code it was found that the MP fields reduce the fast-ion velocity gradients, which drive the GAEs, along the wave-particle resonances in phase space indicating that the GAE drive can be modified with the MP fields.

The reduction of the TAE amplitude was observed with only minor changes in the neutron rate, indicating a lesser role of the fast-ion drive. In this case the TAE suppression was

attributed to changes in the magnetic topology at the plasma edge when the coils are energized. When the MP fields are present the toroidal symmetry is broken and hence, toroidal modes can couple. The STELLGAP code was used to compute the TAE gap in a perturbed magnetic equilibrium and the results indicated that the toroidal mode coupling reduces the TAE gap near the edge, suggesting an increased continuum damping of the observed global TAEs. A more accurate comparison with the experiments, however, requires the inclusion of toroidal rotation effects which were neglected in the STELLGAP simulations presented here.

The observations and the result of the modeling suggest that applied 3D perturbations can be used to effectively control the insurgence of Alfvén instabilities. An effective mitigation scheme has to reduce the mode amplitudes while preserving good fast-ion confinement. In the experiments presented here it was shown that mode amplitudes could be reduced but the fast-ion confinement was compromised.

Although fast-ion transport is very sensitive to 3D fields [50], fine tuning the MP spectrum and amplitude might be possible to obtain a favorable minimum in the fast-ion losses as the MP fields reduce the AE activity and their effects on the fast-ion losses while inducing fast-ion losses themselves. In the current experiments this minimum was not found as indicated by the drop in the neutron rate when the MP fields were applied. In particular, the natural amplification of MP fields provided by the plasma can be exploited to obtain radially localized internal MPs by applying small external fields. In this respect, the possibility of adjusting the radial location of the plasma response by optimizing the MP spectrum and the plasma profiles, in particular the electron diamagnetic frequency, holds interesting possibilities.

While significant theoretical and experimental advances have been seen recently, in the physics of the plasma response to resonant and non-resonant applied MP, dedicated experiments are needed for an accurate study the effect of the MP on AE stability in controlled and well diagnosed scenarios.

Acknowledgments

[1] H.H. Duong, W.W. Heidbrink, E.J. Strait, T.W. Petrie, R. Lee, R.A. Moyer, and J.G. Watkins. (1993) Nucl. Fusion **33** 749

[2] R.B. White, E. Fredrickson, D. Darrow, M. Zarnstorff, R. Wilson, S. Zweben, K. Hill, Yang Chen, and Guoyong Fu. (1995) Phys. Plasmas **2** 2871

[3] B.N. Breizman and S.E. Sharapov. (2011) Plasma Phys. Control. Fusion **53**, 054001

[4] W. W. Heidbrink. (2008) Phys. Plasmas **15** 055501

[5] M. Podestà, W.W. Heidbrink, D. Liu, E. Ruskov, R.E. Bell, D.S. Darrow, E.D. Fredrickson, N.N. Gorelenkov, G.J. Kramer, B.P. LeBlanc, S.S. Medley, A.L. Roquemore, N.A. Crocker, S. Kubota, and H. Yuh (2009) Phys. Plasmas **16** 056104

[6] D. Maslovsky, B. Levitt, and M.E. Mauel. (2003) Phys. Plasmas **10** 1549

[7] D. Maslovsky, B. Levitt, and M.E. Mauel. (2003) Phys. Rev. Lett. **90** 185001

[8] M.A. Van Zeeland, W.W. Heidbrink, R. Nazikian, W.M. Solomon, M.E. Austin, H.L. Berk, N.N. Gorelenkov, C.T. Holcomb, A.W. Hyatt, G.J. Kramer, J. Lohr, M.A. Makowski, G.R. McKee, C.C. Petty, S.E. Sharapov, and T.L. Rhodes (2008) Plasma Phys. Control. Fusion **50**, 035009

[9] K. Nagaoka, T. Ido, E. Ascasîbar, T. Estrada, S. Yamamoto, A.V. Melnikov, A. Cappa, C. Hidalgo, M.A. Pedrosa, B.Ph. van Milligen, I. Pastor, M. Liniers, M.A. Ochando, A. Shimizu, L.G. Eliseev, S. Ohshima, K. Mukai, Y. Takeiri, and the TJ-II Team. (2013) Nucl. Fusion **53** 072004

[10] W.W. Heidbrink, E. Ruskov, E.D. Fredrickson, N.N. Gorelenkov, S.S. Medley, H.L. Berk, and R.W. Harvey. (2006) Plasma Phys. Control. Fusion **48**, 1347

[11] E.D. Fredrickson, G. Taylor, N. Bertelli, D.S. Darrow, D. Liu, and N.A. Crocker, (2014) Proceedings of the 41nd EPS Conference on Plasma Physics and Controlled Fusion , Berlin, volume 29C of *Europhysics Conference Abstracts*, pages P–5.064. The European Physical Society

[12] E.D. Fredrickson, G. Taylor, N. Bertelli, D.S. Darrow, N.N. Gorelenkov, G. Kramer, D. Liu, N.A. Crocker, S. Kubota, and R. White, (2015) Nucl. Fusion **55** 012012

[13] M. Saigusa, H. Kimura, Y. Kusama, G.J. Kramer, T. Ozeki, S. Moriyama, T. Oikawa, Y. Neyatani, and T. Kondoh, (1998) Plasma Phys. Control. Fusion **40**, 1647

[14] S. Bernabei, M.G. Bell, R.V. Budny, E.D. Fredrickson, N.N. Gorelenkov, J.C. Hosea, R. Majeski, E. Mazzucato, C.K. Phillips, G. Schilling, and J.R. Wilson (2000) Phys. Rev. Lett. **84** 1212

[15] G.J. Kramer, C.Z. Cheng, Y. Kusama, R. Nazikian, S. Takeji, and K. Tobita, (2001) Nucl. Fusion **41** 1135

[16] I.T. Chapman (2011) Plasma Phys. Control. Fusion **53**, 013001

[17] Jong-kyu Park, Allen H. Boozer and Alan H. Glasser (2007) Phys. Plasmas **14** 052110

[18] A. Bortolon, W.W. Heidbrink, G.J. Kramer, J.-K. Park, E.D. Fredrickson, J.D. Lore, and M. Podestà, (2013) Phys. Rev. Lett. **110** 265008

[19] M. Ono, S.M. Kaye, Y.-K.M. Peng, G. Barnes, W. Blanchard, M.D. Carter, J. Chrzanowski, L. Dudek, R. Ewig, D. Gates, R.E. Hatcher, T. Jarboe, S.C. Jardin, D. Johnson, R. Kaita, M. Kalish, C.E. Kessel, H.W. Kugel, R. Maingi, R. Majeski, J. Manickam, B. McCormack, J. Menard, D. Mueller, B.A. Nelson, B.E. Nelson, C. Neumeyer, G. Oliaro, F. Paoletti, R. Parsells, E. Perry, N. Pomphrey, S. Ramakrishnan, R. Raman, G. Rewoldt, J. Robinson, A.L. Roquemore, P. Ryan, S. Sabbagh, D. Swain, E.J. Synakowski, M. Viola, M. Williams, J.R. Wilson, and NSTX Team. (2000) Nucl. Fusion **40** 557

[20] R. Maingi, D.P. Boyle, J.M. Canik, S.M. Kaye, C.H. Skinner, J.P. Allain, M.G. Bell, R.E. Bell, S.P. Gerhardt, T.K. Gray, M.A. Jaworski, R. Kaita, H.W. Kugel, B.P. LeBlanc, J. Manickam, D.K. Mansfield, J.E. Menard, T.H. Osborne, R. Raman, A.L. Roquemore, S.A. Sabbagh, P.B. Snyder and V.A. Soukhanovskii (2012) Nucl. Fusion **52** 083001

[21] C.Z. Cheng, (1983) Phys. Rep. **211**, 1

[22] G.J. Kramer, C.Z. Cheng, G.Y. Fu, Y. Kusama, R. Nazikian, T. Ozeki, and K. Tobita, (1999) Phys. Rev. Lett. **83** 2961

[23] J.M. Canik, R. Maingi, T.E. Evans, R.E. Bell, S.P. Gerhardt, B.P. LeBlanc, J. Manickam, J.E. Menard, T.H. Osborne, J.-K. Park, S.F. Paul, P.B. Snyder, S.A. Sabbagh, H.W. Kugel, and E.A. Unterberg (the NSTX Team) (2010) Phys. Rev. Lett. **104** 045001

[24] N.A. Crocker, W.A. Peebles, S. Kubota, J. Zhang, R.E. Bell, E.D. Fredrickson, N.N. Gore-

24

lenkov, B.P. LeBlanc, J.E. Menard, M. Podestà, S.A. Sabbagh, K. Tritz, and H. Yuh. (2011) Plasma Phys. Control. Fusion **53**, 105001

[25] N.N. Gorelenkov, E. Fredrickson, E. Belova, C.Z. Cheng, D. Gates, S. Kaye, and R. White (2003) Nucl. Fusion **43** 228

[26] N.N. Gorelenkov, C.Z. Cheng, E. Fredrickson, E. Belova, D. Gates, S. Kaye, G.J. Kramer, R. Nazikian, and R. White (2002) Nucl. Fusion **42** 977

[27] N.N. Gorelenkov, and C.Z. Cheng, (1995) Nucl. Fusion **35** 1743

[28] W.W. Heidbrink, M.A. Van Zeeland, M.E. Austin, K.H. Burrell, N.N. Gorelenkov, G.J. Kramer, Y. Luo, M.A. Makowski, G.R. McKee, C. Muscatello, R. Nazikian, E. Ruskov, W.M. Solomon, R.B. White, and Y. Zhu (2008) Nucl. Fusion **48** 084001

[29] N. Ferraro and S. Jardin, (2009) J. Comp. Phys. **228** 7742

[30] J. Breslau, N.Ferraro, and S. Jardin, (2009) Phys. Plasmas **16** 092503

[31] N.Ferraro, S. Jardin, and P.B. Snyder, (2010) Phys. Plasmas **17** 092503

[32] L.L. Lao, J.R. Ferron, R.J. Groebner, W. Howl, H. St. John, E.J. Strait, and T.S. Taylor, (1990) Nucl. Fusion **30** 1035

[33] G.J. Kramer, R.V. Budny, A. Bortolon, E.D. Fredrickson, G-Y. Fu, W.W. Heidbrink, R. Nazikian, E. Valeo, M.A. van Zeeland, (2013) Plasma Phys. Control. Fusion **55**, 025013

[34] R.V. Budny, M.G. Bell, A.C. Janos, D.L. Jassby, L.C. Johnson, D.K. Mansfield, D.C. McCune, M.H. Redi, J.F. Schivell, G. Taylor, T.B. Terpstra, M.C. Zarnstorff, and S.J. Zweben (1995) Nucl. Fusion **35** 1497

[35] A. Pankin, D. McCune, R. Andre, G. Bateman, A. Kritz, (2004) Computer Physics Communications **159**, 157

[36] D. Pfefferlé, J.P. Graves, and W.A. Cooper, (2015) Plasma Phys. Control. Fusion **57**, 054017

[37] M.A. Van Zeeland, N.M. Ferraro, B.A. Gierrson, W.W. Heidbrink, G.J. Kramer, C.L. Lasnier, D.C. Pace, S.L. Allen, X. Chen, T.E. Evans, M. García-Muños, J.M. Hanson, M.J. Lanctot, L. Lao, W.H. Meyer, R.A. Moyer, R. Nazikian, D.M. Orlov, C. Pas-Sodan, and A. Wingen, (20015) Nucl. Fusion **55** 073028

[38] W. Kerner, D. Borba, G.T.A. Huysmans, F. Porcelli, S. Poedts, J.P. Goedbloed, and R. Betti, (1994) Plasma Phys. Contr. Fusion **36**, 911

[39] B.P. LeBlanc, R.E. Bell, D.W. Johnson, D.E. Hoffman, D.C. Long, and R.W. Palladino (2003) Rev. Sci. Instrum. **74**, 1659

[40] B.P. LeBlanc, A. Diallo, G. Labik, and D.R. Stevens (2012) Rev. Sci. Instrum. **83**, 10D527

[41] J.D. Huba, (2009) NRL plasma formulary, Naval Research lab. Washington DC

[42] J.-K. Park, A.H. Boozer, A.H. Glasser, (2007) Phys. Plasmas, **14**, 052110

[43] E.D. Fredrickson, N.A. Crocker, D.S. Darrow, N.N. Gorelenkov, G.J. Kramer, S. Kubota, M. Podesta, R.B. White, A. Bortolon, S.P. Gerhardt, R.E. Bell, A. Diallo, B. LeBlanc, F.M. Levinton and H. Yuh (2013) Nucl. Fusion **53** 013006

[44] H.L. Berk, B.N. Breizman, and M. Pekker (1996) Phys. Rev. Lett. **76** 1256

[45] B.N. Breizman, and S.E. Sharapov, (2011) Plasma Phys. Contr. Fusion **53**, 054001

[46] N.N. Gorelenkov, S. Pinches, and k. Toi, (2014) Nucl. Fusion **54** 125001

[47] D.A. Spong, R. Sanchez, and A. Weller. (2013) Phys. Plasmas **10**, 3217

[48] S.P. Hirshman and J.C. Whitson, (1983) Phys. Fluids **26**, 3553

[49] E.D. Fredrickson, N.A. Crocker, R.E. Bell, D.S. Darrow, N.N. Gorelenkov, G.J. Kramer, S. Kubota, F.M. Levinton, D. Liu, S.S. Medley, M. Podestá, K. Tritz, R.B. White, and H. Yuh (2001) Phys. Plasmas **16**, 122505

[50] R.J. Goldston, R.B. White, and A.H. Boozer, (1981) Phys. Rev. Lett. **47**, 647

Princeton Plasma Physics Laboratory
Office of Reports and Publications

Managed by
Princeton University

under contract with the
U.S. Department of Energy
(DE-AC02-09CH11466)